Controlled preparation and detection of d-wave superfluidity in two-dimensional optical superlattices

2009 EPL 87 60001

(http://iopscience.iop.org/0295-5075/87/6/60001)

A Letters Journal Exploring the Frontiers of Physics

September 2009

EPL, **87** (2009) 60001
doi: 10.1209/0295-5075/87/60001

www.epljournal.org

Controlled preparation and detection of d-wave superfluidity in two-dimensional optical superlattices

A. M. Rey[1,2(a)], R. Sensarma[1], S. Fölling[2], M. Greiner[2], E. Demler[2] and M. D. Lukin[2]

[1] *JILA and University of Colorado, Department of Physics, University of Colorado - Boulder, CO 80309, USA*
[2] *Physics Department, Harvard University - Cambridge, MA, 02138, USA*

received 21 August 2009; accepted 12 September 2009
published online 28 September 2009

PACS 03.75.Ss – Degenerate Fermi gases
PACS 37.10.Jk – Atoms in optical lattices
PACS 74.20.Mn – Nonconventional mechanisms (spin fluctuations, polarons and bipolarons, resonating valence bond model, anyon mechanism, marginal Fermi liquid, Luttinger liquid, etc.)

Abstract – d-wave Cooper pairs are believed to be the key for understanding the phenomenon of high-temperature superconductivity in cuprates. These superconductors are an example of the emergence of strong pairing in systems with purely repulsive interactions, similar to superfluid helium 3 and the newly discovered iron oxypnictides. Despite intense studies, there is currently no consensus as to what causes the formation of d-wave Cooper pairs in these materials. Here we propose a novel experimental scheme in which recently demonstrated methods for realizing optical lattices and superlattices are combined to create and to detect, in a controlled way, ultracold-atom d-wave Cooper pairs. Our scheme starts from arrays of isolated plaquettes which incorporate the required d-wave correlations on a short length scale. By tuning the parameters of the potentials, these plaquettes can be coupled to achieve long-range d-wave superfluid correlations, finally arriving at the generic Hubbard model.

Introduction. – The "pure" 2D repulsive Hubbard model is a simple lattice model in which fermionic particles move between sites by tunnel coupling and repel each other when they occupy the same site. It has long been suggested as a model which might contain the basic physics required to explain the high temperature superconductivity observed in cuprates and similar materials. For the Hubbard model, d-wave pairing is expected to occur from an effective attraction caused by the exchange of spin fluctuations [1]. Nonetheless, whether this pairing can give rise to long-range order and superconductivity it is still unknown [2–4]. Recent experimental breakthroughs in the field of ultracold atoms loaded into optical lattices [5,6] such as the observation of the superfluid to Mott insulator transition with bosons [7] and the experimental realization of both repulsive and attractive Hubbard models [8–10] with fermions suggest that ultracold atoms are uniquely suited to experimentally address these open questions.

Here we propose a method for the controlled preparation and detection of atomic d-wave superfluidity using optical superlattices. The method is based on two experiments which together connect the known d-wave symmetry of fermions in a single plaquette [11] —four lattice sites arranged in a square— (fig. 1(a)) with the unknown d-wave properties of the generic 2D Hubbard model. Both of the experiments use demonstrated and currently available tools and techniques. A pair of weakly coupled plaquettes is the simplest system which exhibits a specific range of parameters where two holes tend to bind together on a single plaquette rather than to delocalize among the two [12–17]. The hole pair or Cooper pair that is created has a d-wave symmetry and leads to d-wave superfluidity once many plaquettes are weakly coupled [12–14]. In the first experiment we propose to use coherent dynamics to probe the formation of d-wave Cooper pairs and their binding energy. The basic idea is to load single plaquettes with specific number of fermions and then weakly connecting pairs of adjacent plaquettes into a superplaquette (fig. 1(b)). The second experiment consists of weakly connecting the plaquettes into a 2D array (checkerboard

(a) E-mail: arey@jilau1.colorado.edu

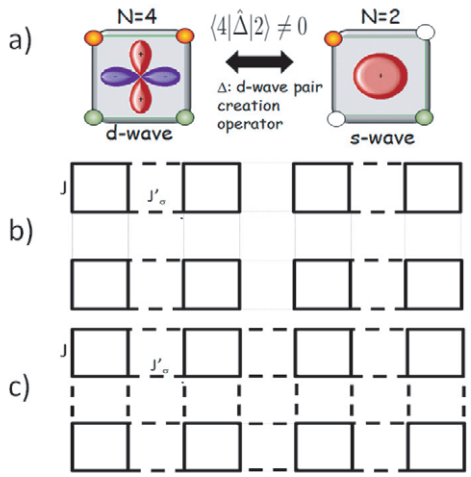

Fig. 1: (Color online) A plaquette is the minimum system that exhibits d-wave symmetry. a) When loaded with four fermions the ground state is d-wave symmetric while when loaded with 2 the ground state exhibits s-wave symmetry. Consequently, the two states have a non-zero matrix element with the d-wave pair creation operator. Here we consider the situations where plaquettes are coupled into a superplaquette array and into a checkerboard array, which are schematically represented in b) and c), respectively. In the picture the spin-independent intra-plaquette tunneling J is represented by a thick solid line and the inter-plaquette tunneling, $J'_\sigma \ll J$ by a dashed line. The subscript σ in J'_σ emphasizes that it can depend on the spin of the atom.

array, fig. 1(c)) and study their long-range d-wave correlations. The manipulations required to implement these schemes rely on the large degree of control which is available in ultracold atom systems. They will enable a experimental confirmation of induced pairing resulting from purely repulsive Hubbard physics. In a final step, the weak coupling between the plaquettes is increased until a regular 2D square lattice is created. The overall procedure opens a unique possibility to continuously connect a known d-wave coupling mechanism to the unknown case of the 2D square lattice Hubbard model.

The phase diagram of the checkerboard lattice, realized in the second experiment, is very rich, as recently demonstrated in refs. [12–14]. In the parameter regime of our interest it exhibits a d superfluid phase and a Cooper pair density wave state which is conceptually similar to a charge density wave phase. Here we derive the phase diagram for the homogeneous system in the general case of spin-dependent inter-plaquette tunneling, which is experimentally realizable with cold atoms. In addition we use the local density approximation to study the quantum phases in the presence of an additional parabolic confinement which is typically present in all experimental realizations.

To prepare and analyze the states we combine a number of recently demonstrated techniques which use the tunability of laser parameters [18] and noise correlation measurements [19–23]. The latter method is used specifically for the characterization of the quantum phases in the checkerboard array. The overall description takes into account important experimental details such as the number of required lattice periodicities and the availability of required laser sources, and considers experimental constraints such as inhomogeneous trapping potentials. We also discuss the requirements for temperature and adiabaticity of state preparation, which are crucial factors for any realistic implementation.

Step I: plaquette fermion models

Hamiltonian. We consider fermions in an isolated plaquette (shown in fig. 1(a)). Assuming one accessible single particle state in each well (*i.e.* level spacing much larger than other energy scales in the problem), the system is described by the Hubbard Hamiltonian

$$\hat{H} = -J \sum_{\langle r,r'\rangle,\sigma} \hat{c}^\dagger_{r\sigma}\hat{c}_{r'\sigma} + U\sum_r \hat{n}_{\uparrow r}\hat{n}_{\downarrow,r}, \qquad (1)$$

where J is the tunneling matrix element and U is the onsite Hubbard repulsion. Here $\hat{c}_{r\sigma}$ are fermionic annihilation operators, $\hat{n}_{r\sigma} = \hat{c}^\dagger_{r\sigma}\hat{c}_{r\sigma}$ are number operators, $r = 1,\ldots,4$, labels the four sites in a plaquette and the term $\langle r, r'\rangle$ indicates that the sum is restricted to nearest neighbors.

The eigenstates in a single plaquette depend on the filling factor. When filled with $N = 4$ or $N = 2$ fermions, the ground state is a spin-singlet exhibiting d- and s-wave symmetry, respectively. We denote the corresponding ground states as $|4\rangle$ and $|2\rangle$ (see fig. 1(a)). On the other hand, for $N = 3$, the ground state is degenerate with $S = 1/2$ and $p_x \pm ip_y$ symmetry in the regime $U < U_t \sim 18.6J$. We denote them as $|3^{(\sigma,\tau)}\rangle$ with σ and τ specifying the spin polarization and the orbital "chirality" ($\tau = \pm$). The d- *vs.* s-wave symmetry of the $|4\rangle$ and $|2\rangle$ states is the crucial element in obtaining the d-wave pairing mechanism, since the hole-pair creation operator that connects the two states must have a d-wave symmetry [11]; *i.e.* $\langle 2|\hat{\Delta}^\dagger_d|4\rangle \neq 0$, where

$$\hat{\Delta}_d = (\hat{s}_{12} + \hat{s}_{34} - \hat{s}_{14} - \hat{s}_{23})/2, \qquad (2)$$

and $\hat{s}_{rr'} = (\hat{c}^\dagger_{r\uparrow}\hat{c}^\dagger_{r'\downarrow} - \hat{c}^\dagger_{r\downarrow}\hat{c}^\dagger_{r'\uparrow})/\sqrt{2}$ creates a singlet on the rr' bond.

We next look at the case of 2 holes in two isolated plaquettes. The holes can bind together within the same plaquette or separate as single holes in each plaquette depending on the binding energy defined as

$$\Delta_b = 2E_g(N = 3) - E_g(N = 4) - E_g(N = 2) \qquad (3)$$

being positive or negative, respectively. Here $E_g(N = n)$ is the single plaquette ground-state energy when loaded with n atoms. As shown in fig. 2, Δ_b is a non-monotonic function of U/J [12–14,16,17,24], which reaches a maximum value of $\Delta_b \approx 0.04J$ at $U \approx 2.45J$ and becomes negative for $U = U_c > 4.58J$. Consequently, only when $U < U_c$ hole pairs on a single plaquette are energetically stable.

Two adjacent plaquettes can be coupled through a weak (possibly spin-dependent) tunneling J'_σ to form a

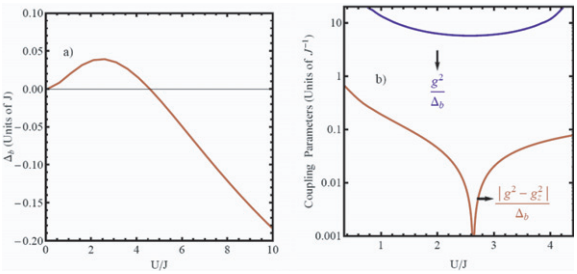

Fig. 2: (Color online) Pair binding energy and inter-plaquette coupling strengths of the effective XXZ Hamiltonian, eq. (5). a) The red solid line corresponds to the pair binding energy in a plaquette. For $0<U/J<4.6$, $\Delta_b>0$ and consequently it is energetically favorable to have two holes in the same plaquette. b) Effective XXZ coupling parameters as a function of U/J. The blue line corresponds to g^2/Δ_b as a function of U/J. This is the only parameter that appears in the superplaquette Hamiltonian. When more than two plaquettes are coupled, new virtual processes have to be accounted for, which change the Ising term coupling constant. While the latter become proportional to g_z^2/Δ_b, the transverse coupling constant remains the same, *i.e.* proportional to g^2/Δ_b. The red line shows the absolute value of the difference between these two parameters.

superplaquette (see fig. 1). As long as $0<J'_\sigma\ll\Delta_b$, the states $|4,2\rangle$ and $|2,4\rangle$ are lower in energy and occupation of the states $|3^{(\sigma,\tau)},3^{(\bar\sigma,\bar\tau)}\rangle$ are energetically suppressed. They can only be populated as "virtual" intermediate states leading to an effective superexchange interaction between $|4,2\rangle$ and $|2,4\rangle$. Specifically, by treating the $|4\rangle$ and $|2\rangle$ states as the pseudo-spin components $|\Uparrow\rangle$ and $|\Downarrow\rangle$ of an effective spin-1/2 system, the interaction between the effective spins can be described by an XXZ-type Hamiltonian

$$H_{eff}=-\frac{J'_\uparrow J'_\downarrow g^2}{\Delta_b}(\sigma_R^x\sigma_L^x+\sigma_R^y\sigma_L^y)+\frac{g^2(J'^2_\uparrow+J'^2_\downarrow)}{2\Delta_b}\sigma_R^z\sigma_L^z \tag{4}$$

with $\sigma_{i=R,L}^{\alpha=x,y,z}$ standard Pauli matrices acting on the right (R) or left (L) effective pseudo-spins and g the coupling matrix element between the right and left plaquettes which is of order one (see fig. 2).

Equation (4) contains the essential physics we are interested for this work. If $J'_\uparrow=J'_\downarrow$ the energy eigenstates are effective triplet and singlet states $|t,s\rangle=\frac{1}{\sqrt{2}}(|4,2\rangle\pm|2,4\rangle)$ with the triplet being the ground state. These are separated by an energy gap $\sim\Delta_b$ from the rest of the Hilbert space. The ground state has a non-zero expectation value of the d-wave pair correlation operator $\langle t|\hat\Delta_d^\dagger(R)\hat\Delta_d(L)|t\rangle\neq0$ which leads to a d-wave superfluid when coupling all the plaquettes. Here $\hat\Delta_d^\dagger(R,L)$ is the d-wave operator, eq. (2), evaluated at the right or left plaquettes. On the contrary if $J'_\uparrow\ll J'_\downarrow$, the Ising term dominates and any infinitesimal symmetry-breaking perturbation will collapse the state into $|4,2\rangle$ or $|2,4\rangle$ which are inherently density-ordered states. These considerations indicate that the many-body phase diagram of this model would depend on the spin-dependent couplings in a non-trivial way.

Preparation and detection. To verify the energy structure of the hole-pair states we want to create an array of isolated superplaquettes loaded with 2 and 4 fermions in the left and the right plaquettes, respectively.

An array of plaquettes can be created by combining two orthogonal optical superlattices formed by the superposition of two independent sinusoidal potentials which differ in periodicity by a factor of two [18,25–28]. The aim here is first to load the fermions in a 2D array of independent plaquettes with alternating filling factors of 4 and 2 along one direction. The preparation procedure we propose is based on a unity-filled band insulator [29], and uses adiabatic manipulations of a superlattice potential created by standing waves with four different periodicities λ, 2λ, 4λ and $4\lambda/3$. For other strategies see [17]. Such wavelength combinations and the appropriate sources are available for typical fermionic atoms such as ^{40}K and ^{6}Li (for example with $\lambda=532$ nm in the case of ^{40}K). The required geometries can also be engineered with a single laser source, by intersecting pairs of laser beams propagating in the 2D plane with appropriate angles [30], resulting in a set of four equidistant k-vectors along the x-axis. For the discussion we will also assume that there is a deep axial lattice that freezes the atom motion along the z-direction.

The process of patterned loading an array of plaquettes is presented in fig. 3. Additional spin-dependent control of the inter-plaquette tunneling can be achieved by controlling the laser polarizations [26]. After the tunnel coupling between the two plaquettes has been enabled, the system will exhibit coherent Rabi oscillations between $|4,2\rangle$ and $|2,4\rangle$ states with the $|3,3\rangle$ populated virtually (see fig. 4). The frequency of oscillation of the envelope is given by $4g^2J'^2/\Delta_b$ and can be used to measure the binding energy of the hole pairs. These ideas are similar to the ones used to measure the superexchange energy in an array of double wells [31]. To measure the number of superplaquettes in $|4,2\rangle$, $|2,4\rangle$ and $|3,3\rangle$ states one can use band-mapping techniques [32].

Step II: checkerboard lattice. – The second experiment brings us one step forward towards the generic 2D system. It consists on weakly coupling the plaquettes into a 2D checkerboard pattern such as the one shown in fig. 1(c).

We will restrict our analysis to the regime $|\Delta_b|\gg gJ'_\sigma$ and $\Delta_b>0$ where we can treat the states $|2\rangle$ and $|4\rangle$ as the low energy modes and adiabatically eliminate high energy states via second-order perturbation theory. This procedure yields a more general effective XXZ Hamiltonian given by

$$H_{eff}=\sum_{\langle\mathbf{R},\mathbf{R}'\rangle,\mathbf{u}=\mathbf{x},\mathbf{y},\mathbf{z}}J^u\sigma^u_{\mathbf{R}}\sigma^u_{\mathbf{R}'}-\mu_z\sum_{\mathbf{R}}\sigma^z_{\mathbf{R}}, \tag{5}$$

where $J^{x,y}=-J^\perp=\frac{g^2J'_\uparrow J'_\downarrow}{\Delta_b}$, $J^z=(J'^2_\uparrow+J'^2_\downarrow)\frac{g_z^2}{2\Delta_b}$. The coupling matrix element g_z has a complicated dependence

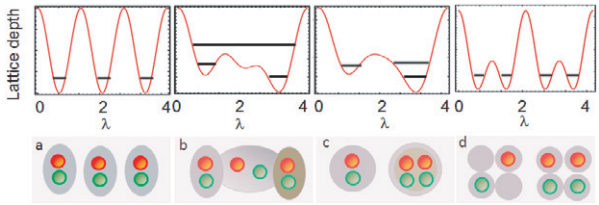

Fig. 3: (Color online) Patterned loading of fermions into an array of plaquettes: a) the initial band insulator is formed in a rectangular lattice generated by light with wavelengths $4/3\lambda$ and 2λ along the x and y directions, respectively. b) Adiabatically introducing a phase shifted 4λ lattice along the x-axis creates an effective 4λ lattice with three sites per cell with different energy offsets. c) By ramping down the period $4/3\lambda$ lattice while ramping up the period 2λ one can convert the potential into a double-well lattice with an asymmetric energy offset. This offset has to be large compared to the on-site repulsion to guarantee that the final ground state corresponds to a system with four fermions in the lower and two fermions in the higher sites of each double well. d) After increasing the lattice depth of the 2λ lattice to suppress tunneling between the wells the bias can be removed and the isolated wells can be split into four sites by slowly turning on the λ lattice along both x and y directions. As a result, an array of independent plaquettes in the ground state with alternating filling factors of 4 and 2 along the x-direction is created. To obtain an array of superplaquettes, the tunneling between adjacent plaquettes can be controlled by the depth of the 2λ potential, while the 4λ lattice intensity controls the suppression of tunneling between superplaquettes. The $4\lambda/3$ lattice is used to balance site energy offsets created when the long lattice is added.

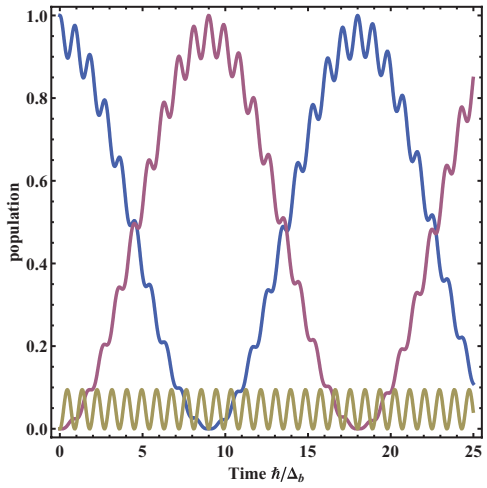

Fig. 4: (Color online) Time evolution of the populations of superplaquettes in the three lowest-energy states after preparation in the state $|4,2\rangle$. The populations $N_{42}(t)$, $N_{24}(t)$ and $N_{33}(t)$ are shown in blue, purple and ochre, respectively. The fast frequency component is determined by Δ_b and the slow envelope by $J'^2\, g^2/\Delta_b$. Here $U/J=2.6$ and $J'/J=0.01$.

on U/J as shown in fig. 2. Here we have introduced an effective chemical potential μ_z (or energy of adding two atoms to a plaquette). In the effective spin picture it can

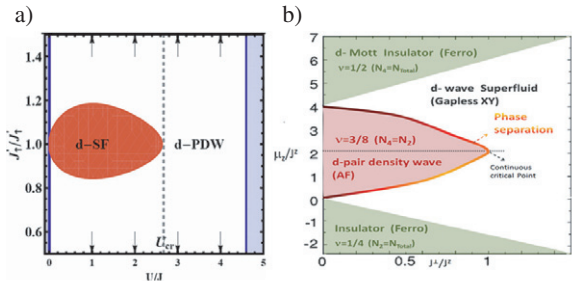

Fig. 5: (Color online) a) Zero-temperature phase diagram at 3/8 fermionic filling ($N_4=N_2=N_{total}/2$). At this filling the system exhibits a second-order phase transition from a d-wave superfluid, d-SF (magnetic ordered state in the XY-plane for the effective spins) to a d-pair density wave state, d-pdw (anti-ferromagnetic ordered phase for the effective spins) when the axial, J^z, and the transverse $J^\perp$, coupling constants that appear in the XXZ Hamiltonian become equal. As both $J^\perp$ and J^z depend on the inter-plaquette tunnelings $J'_{\uparrow,\downarrow}$ and the ratio U/J, the critical point can be controlled by tuning these microscopic parameters. b) Zero-temperature phase diagram of the effective XXZ Hamiltonian as a function of an effective chemical potential, μ_z, adapted from ref. [34]. μ_z accounts for the energy of adding two atoms to a plaquette, and can be visualized as an effective magnetic field in the effective spin picture. The phase diagram has a lobe-like structure: Inside the $\nu=3/8$ lobe the system is d-pdw. Outside it the system enters a gapless d-wave superfluid phase or an insulating phase depending on the value of the effective chemical potential. In the insulating phases the density is fixed to $\nu=1/2$ ($N_4=N_{total}$) or $\nu=1/4$ ($N_2=N_{total}$). The transition from a d-pdw to a d-wave superfluid is a first-order phase transition (except at the tip which corresponds to the $J^\perp=J^z$ critical point) and induces phase separation in a small range of filling factors around $N_4=N_2$.

be thought of as an effective external magnetic field along the z-direction.

The zero-temperature phase diagram of the XXZ Hamiltonian is known and consequently can be used to infer the phase diagram of the corresponding fermionic system [12–14,33,34]. At $\nu=3/8$ fermionic filling, *i.e.* $N_4=N_2$, there is a second-order phase transition which belongs to the XY universality class as the $J^z/J^\perp$ ratio is varied: while for $J^z/J^\perp<1$ the ground state corresponds to a gapless d-wave superfluid (a magnetically ordered phase in the XY-plane for the effective spins), for $J^z/J^\perp>1$ it becomes a gapped Cooper pair density wave state, d-pdw (an anti-ferromagnetic order phase for the effective spins). The pdw state is not the usual particle-hole charge density wave state, but can be viewed as a crystal of d-wave Cooper pairs [35]. The point $J^z=J^\perp$ is the critical point. In fig. 5(a), we show the phase diagram as a function of $J'_\uparrow/J'_\downarrow$ where the tendency of anisotropic tunneling to stabilize the d-pdw phase can be observed. For the spin-independent case $J'_\uparrow=J'_\downarrow$, our phase diagram is in agreement with the one obtained in ref. [14], exhibiting a critical point at $U_c\sim 2.7J$. Notice that since our analysis is based on the assumption that

$gJ' \ll \Delta_b$, the parameter regime where it is applicable considerably reduces as one approaches the points $U = 0$ and $U/J \sim 4.6$, where Δ_b vanishes.

Away from the fermionic filling $\nu = 3/8$ and provided the number of fermions per plaquette is between 2 and 4, $1/4 < \nu < 1/2$, which is required for the validity of the effective XXZ Hamiltonian, the phase diagram is almost insensitive to the $J'_\uparrow/J'_\downarrow$ ratio. There is a first-order phase transition from the d-pdw phase to the d-wave superfluid as the effective chemical potential is varied away from $\nu = 3/8$ filling. Due to the first-order character of the transition, the d-pdw phase is surrounded by a small region where one observes phase coexistence [34]. Outside this region, the low energy phase is always a gapless d-wave superfluid except from the case where $N_4 = N_{total}$ or $N_2 = N_{total}$ where the system turns into an insulator.

When plotted as a function of the effective chemical potential [34], the phase diagram has a characteristic lobe-like structure, which can be understood by mapping the effective XXZ spin model to a hard-core bosons extended Bose Hubbard model with tunneling $J = J^\perp/2$ and nearest-neighbor interactions $V = J^z$. In this visualization of the phase diagram the tip of the d-pdw lobe corresponds to the critical Heisenberg point.

So far we have discussed the zero-temperature homogeneous case, however, in most cold atom experiments there is also a parabolic confinement present and the temperature is not exactly zero. In the remainder of this section we discuss both issues.

Within each plaquette, the external parabolic potential adds a term in eq. (1) equal to $\Omega \sum_r R_r \hat{n}_r + \Omega \mathbf{R}^2 N_R$, with $\Omega = \frac{1}{2} M \omega_t^2 \lambda^2$, M the atom mass, $\mathbf{R} = (2i, 2j)$ the coordinates of the center of the plaquette in lattice units, i, j integers and $R_r = (\pm 2i, \pm 2j)$. The first term, $\Omega \sum_r R_r \hat{n}_r$ breaks the symmetry within the four sites of the plaquette and directly affects the magnitude of the binding energy. We find that Δ_b is a very sensitive quantity, however for example for ^{40}K atoms, by using a weak transversal parabolic confinement of $2\pi \times 20\,\mathrm{Hz}$ one could achieve a reduction in Δ_b less than 5%, for $1 < U/J < 3$, within a radius of the order of 20 lattice sites, *i.e.* $\sqrt{|i|^2 + |j|^2} < 20$. Provided high fidelity preparation, the 5% variations will not significantly degrade the measurements of the binding energy using the superplaquette dynamics. The second term, $\Omega \mathbf{R}^2 N_R$ modifies globally the energy of each plaquette and can be accounted for by adding an effective position dependent chemical potential to the effective Hamiltonian, $\mu_z \to \mu_z(\mathbf{R}) = \bar{\mu}_z - \Omega \mathbf{R}^2$, with $\bar{\mu}_z$ a global effective chemical potential. The latter generates a shell structure consisting on d-wave Mott phases–d-wave SF–d-pdw–d-wave SF and band insulator phases as ones moves from the center of the trap to the edges. The phase at the center of the trap is determined by $\bar{\mu}_z$ which can be controlled by the superplaquette preparation procedure.

To estimate an upper bound of the temperature of the initially trapped Fermi gas required for observing the phase diagram (assuming all later modifications are adiabatic) we use well known results from the effective spin Hamiltonian [36,37] (see appendix). We obtain that the initial temperature must be below $T/T_F \sim 0.01$ to observe the quantum phases. Here T_F is the Fermi temperature of the initially trapped gas. This value even though small is close to being achieved in current experiments.

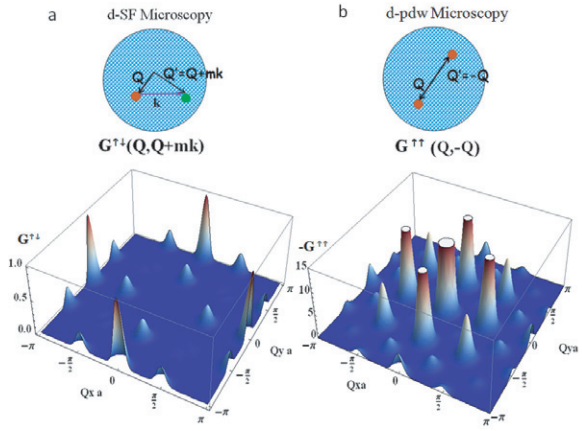

Fig. 6: (Color online) The left panels display the unequal spin noise correlations, $G^{\uparrow\downarrow}(\mathbf{Q}, \mathbf{Q}' = \mathbf{Q} + m\mathbf{k})$, where $\mathbf{k} = 2\pi/\lambda \hat{x}$ is the reciprocal lattice vector of the underlying lattice with spacing λ, assuming a d-wave superfluid. The right panel shows equal spin noise correlations (with opposite sign) $-G^{\uparrow\uparrow}(\mathbf{Q}, \mathbf{Q}' = -\mathbf{Q})$ for a d-pdw state. Here we have subtracted the local density-density correlations within a plaquette. $G^{\uparrow\downarrow}(\mathbf{Q}, \mathbf{Q}')$ exhibits interference peaks at $\mathbf{Q} + \mathbf{Q}' = \mathbf{K}n$ in the d-wave superfluid regime with $\mathbf{K} = \mathbf{k}/2$ is the reciprocal lattice vector of the plaquette array. The peaks are modulated by an overall envelope which probes the d-wave symmetry. This modulation causes the disappearance of the peaks along the nodal lines $Q_x = \pm Q_y$. On the contrary $-G^{\uparrow\uparrow}(\mathbf{Q}, \mathbf{Q}')$ exhibits interference peaks at $\mathbf{Q} - \mathbf{Q}' = \mathbf{K}(2n+1)/2$ in the d-pdw state. Due to the large kinetic energy of the fermions within a plaquette these peaks however are much weaker than the anti-bunching peaks, which always appear at $\mathbf{Q} - \mathbf{Q}' = n\mathbf{K}$.

Detection via Noise correlations. – Noise correlations [23] can be used to detect the different quantum phases.

The second-order correlation function of the noise in an expanding cloud is related to the following four point functions at the time of the release:

$$G^{\sigma\sigma'}_{\mathbf{Q},\mathbf{Q}'} \propto \langle \hat{n}_{\mathbf{Q}\sigma} \hat{n}_{\mathbf{Q}'\sigma'} \rangle - \langle \hat{n}_{\mathbf{Q}\sigma} \rangle \langle \hat{n}_{\mathbf{Q}'\sigma'} \rangle \qquad (6)$$

with $\hat{n}_{\mathbf{Q}\sigma} \propto \sum_{l,s} e^{i\mathbf{Q}\cdot(\mathbf{L}_{ls})} \langle c^\dagger_{l\sigma} c_{s\sigma} \rangle$, being the quasi-momentum distribution and $\mathbf{L}_{ls}$ a vector connecting the lattice sites s and l. $G^{\sigma\sigma'}(\mathbf{Q}', \mathbf{Q})$ has the required ingredients to distinguish the two phases. On the one hand, $G^{\uparrow\downarrow}(\mathbf{Q}, \mathbf{Q}')$ contains terms proportional to $\langle \hat{\Delta}^\dagger_d \hat{\Delta}_d \rangle$ (see eq. (2)), and consequently a d-wave superfluid with $\langle \hat{\Delta}_d \rangle \neq 0$ must exhibit interference fringes at $\mathbf{Q} + \mathbf{Q}' = \mathbf{K}n$. Here, $\mathbf{K}$ is the reciprocal lattice vector of the plaquette array, which is half of the reciprocal lattice vector of the underlying lattice. The d-wave nature of the state will be signaled by a modulation of the peaks with an a overall envelope with the characteristic d-wave nodal planes along $Q_x = \pm Q_y$ and $Q'_x = \pm Q'_y$ as shown in fig. 6.

Information about the density order is given by $G^{\uparrow\uparrow}$ which will show sharp dips at $\mathbf{Q}-\mathbf{Q}'=(2n+1)\mathbf{K}/2$ in the presence of a d-pdw phase and a flat profile in the superfluid phase. In contrast to the unequal spin correlations, $G^{\uparrow\uparrow}$ will not have the inherent d-wave symmetry. Equal spin correlations will also always exhibit dips at $\delta(\mathbf{Q}-\mathbf{Q}'-n\mathbf{K})$ which reflect the characteristic anti-bunching of fermions [22]. Unfortunately, the amplitude of these dips can be about 30 times stronger than the dips at $(2n+1)\mathbf{K}/2$ inherent from the charge density order (see fig. 6(b)). This caveat can be avoided by slowly merging each plaquette into a single well before the release which will map the d-pdw into a charge density phase of frozen atoms (with alternating filling factors of four and two).

Conclusions. – In summary, we described a pair of experiments to prepare and detect d-wave superfluidity in ultracold fermionic atoms loaded into optical superlattices. The experimental schemes are based on current techniques and together provide a continuous path from a theoretically predictable, but not yet observed, d-wave superfluid phase arising from repulsive interactions to the unknown d-wave coupling properties of the 2D Hubbard model phase diagram. Our analysis takes experimental constraints such as parabolic confinements into account and suggests that the scheme works for typical experimental geometries.

* * *

This work was supported by ITAMP, NSF (Career Program, frontier in Physics), Harvard-MIT CUA, AFOSR, Swiss NF, the Sloan Foundation, and the David and Lucille Packard Foundation.

Appendix: temperature estimation. – To estimate an upper bound of the required initial T/T_F of a trapped Fermi gas for observing the characteristic XXZ phase diagram we assume adiabatic loading and equate the entropy of the trapped Fermi gas to the entropy at criticality of the effective spin Hamiltonian considering two limiting cases: a pure 2D anti-ferromagnetic Ising regime and a pure XY model regime. We expect this treatment can provide fair temperature estimates expect from the path at the tip of the lobe where $T_c=0$. The 2D Ising Hamiltonian has an exact solution developed by Onsager [36] which predicts $kT_c=2.26\,J^z$ and an entropy per particle at T_c, $S(T_c)=0.3k$, here k is the Boltzmann constant. The XY Hamiltonian is not exactly solvable but Monte Carlo simulations [37] have predicted a BKT critical temperature of $kT_c=0.353\,J^{\perp}$ and a specific heat of $C_v=1.78\,T^2k^3/J^{\perp 2}$ for $kT<0.4\,J^{\perp}$. Using these results one can calculate an entropy per particle at T_c equal to $S(T_c)=0.1k$. Equating these final entropies to the one of a 3D trapped degenerated Fermi gas $S=k\pi^2\,T/T_F$ one gets that the required initial T/T_F has to be less than 0.03 and 0.01 for the pure d-pdw and d-SF, respectively, being the former the one that imposes the strongest restriction.

REFERENCES

[1] Anderson P. W., *Phys. Scr.*, **T102** (2002) 10.
[2] Scalapino D. J, in *Handbook of High-Temperature Superconductivity*, edited by Schrieffer J. R. and Brooks J. S. (Springer, New York) 2007.
[3] Dagotto E., *Rev. Mod. Phys.*, **66** (1994) 763.
[4] Bednorz J. G. and Muller K. A., *Z. Phys. B*, **64** (1986) 189.
[5] Bloch I., Dalibard J. and Zwerger W., *Rev. Mod. Phys.*, **80** (2008) 885.
[6] Greiner M. and Folling S., *Nature*, **453** (2008) 736.
[7] Greiner M. *et al.*, *Nature*, **415** (2002) 39.
[8] Strohmaier N. *et al.*, *Phys. Rev. Lett.*, **99** (2007) 220601.
[9] Jördens R. *et al.*, *Nature (London)*, **455** (2008) 204.
[10] Schneider U. *et al.*, *Science*, **322** (2008) 1520.
[11] Scalapino D. J. and Trugman S. A., *Philos. Mag. B*, **74** (1996) 607.
[12] Tsai W. F. and Kivelson S. A., *Phys. Rev. B*, **73** (2006) 214510.
[13] Tsai W. F., Yao H., Laeuchli A. and Kivelson S. A., *Phys. Rev. B*, **77** (2008) 214502.
[14] Yao H., Tsai W. F. and Kivelson S. A., *Phys. Rev. B*, **76** (2007) 161104R.
[15] Morningstart C. J. and Weinstein M., *Phys. Rev. D*, **54** (1996) 4131.
[16] Altman E. and Auerbach A., *Phys. Rev. B*, **65** (2002) 104508.
[17] Trebst S., Schollwöck U., Troyer M. and Zoller P., *Phys. Rev. Lett.*, **96** (2006) 250402.
[18] Trotzky S. *et al.*, *Science*, **319** (2008) 295.
[19] Altman E., Demler E. and Lukin M. D., *Phys. Rev. A*, **70** (2004) 013603.
[20] Fölling S. *et al.*, *Nature*, **434** (2005) 481.
[21] Greiner M. *et al.*, *Phys. Rev. Lett.*, **92** (2004) 150405.
[22] Rom T. *et al.*, *Nature*, **444** (2006) 73.
[23] Spielman I., Phillips W. D. and Porto J. V., *Phys. Rev. Lett.*, **98** (2007) 080404.
[24] Schumann R., *Ann. Phys. (Leipzig)*, **11** (2002) 49.
[25] Paredes B. and Bloch I., *Phys. Rev. A*, **77** (2008) 023603.
[26] Sebby-Strabley J., Anderlini M., Jessen P. S. and Porto J. V., *Phys. Rev. A*, **73** (2006) 033605.
[27] Fölling S. *et al.*, *Nature*, **448** (2007) 1029.
[28] Cheinet P. *et al.*, *Phys. Rev. Lett.*, **101** (2008) 090404.
[29] Köhl M. *et al.*, *Phys. Rev. Lett.*, **94** (2005) 080403.
[30] Peil S. *et al.*, *Phys. Rev. A*, **67** (2003) 051603R.
[31] Rey A. M. *et al.*, *Phys. Rev. Lett.*, **99** (2007) 140601.
[32] Anderlini *et al.*, *J. Phys. B*, **39** (2006) S199.
[33] Batrouni G. G. and Scalettar R. T., *Phys. Rev. Lett.*, **84** (2000) 1599.
[34] Hebert F. *et al.*, *Phys. Rev. B*, **65** (2001) 014513.
[35] Chen H. D., Vafek O., Yazdani A. and Zhang S. C., *Phys. Rev. Lett.*, **93** (2004) 187002.
[36] Onsager L., *Phys. Rev.*, **65** (1944) 117.
[37] Ding H. Q., *Phys. Rev. B*, **45** (1992) 230.